EFFECT OF FLOW SEPARATION OF TiO_2 NANOFLUID ON HEAT TRANSFER IN THE ANNULAR SPACE OF TWO CONCENTRIC CYLINDERS

by

Tuqa ABDULRAZZAQ [a]***, Hussein TOGUN*** [b*]***, Mohammad REZA SAFAEI*** [c,d]***,***
Salim Newaz KAZI [e]***, Mohd Khairol Anuar bin Mohd ARIFFIN*** [f]***,***
and Nor Mariah ADAM [f]

[a] Petroleum and Gas Engineering Department, University of Thi-Qar, Nassiriya, Iraq
[b] Biomedical Engineering Department, University of Thi-Qar, Nassiriya, Iraq
[c] Division of Computational Physics, Institute for Computational Science, Ton Duc Thang University, Ho Chi Minh City, Vietnam
[d] Faculty of Electrical and Electronics Engineering, Ton Duc Thang University, Ho Chi Minh City, Vietnam
[e] Mechanical Engineering Department, University of Malaya, Kuala Lumpur, Malaysia.
[f] Mechanical and Manufacturing Engineering Department, Universiti Putra Malaysia, Selangor, Malaysia

Original scientific paper
https://doi.org/10.2298/TSCI180709321A

In the wake of energy crises, the researchers are encouraged to explore new ways of enhancement in the thermal performance of heat exchanging equipment. In the current research, the SST k-ω model and finite volume method were employed to augment heat transfer into the separation flow of TiO_2 nanofluid in the annular space of two concentric cylinders. In the present investigation TiO_2 nanoparticles of volume fractions, 0.5%-2% at Reynolds number range of 10000-40000, and contraction ratios from 1 to 2 were considered at constant heat flux boundary condition. Simulation results reveal that the highest enhancement in the heat transfer coefficient is corresponding to the annular pipe with a contraction ratio of 2 due to the generated re-circulation flow zone that begins after the separation point on the wall. Further, the surface heat transfer coefficient enhances with the increase of nanoparticles volume fraction and Reynolds number. The velocity distribution profile before and after the steps reveals that increasing the height of the step and Reynolds number, re-circulation regions also increases. Numerical results indicate that the highest pressure drop occurs at the Re = 40000 and contraction ratio of 2.

Key words: *nanofluids, re-circulation flow, abrupt contraction, concentric cylinders, separation flow*

Introduction

Heat transfer enhancement methods were widely investigated by numerous researchers in the recent past who explored the effect of geometry (such as micro-channel, mini-channel, tube*, etc.*) on the heat transfer coefficient for the flow in a sudden expansion or contraction of

* Corresponding author, e-mail: htokan_2004@yahoo.com

backward or forward-facing steps or on ribbed channels. Abu-Mulaweh [1] studied the turbulent heat transfer of air-flow over a vertical forward-facing step experimentally. They also studied the influence of the height of step on the distribution of local Nusselt number and declared that the local Nusselt number enhances with the augmentation of the height of step in the reattachment point. By employing the k-ε turbulence model, Orselli and Lemos [2] numerically simulated the turbulent flow and heat transfer through a sudden contraction with porous insert and indicated that porous insert leads to the reduction of circulation region. Nassab *et al.* [3] numerically studied the efficacy of step height and slope angle on flow and heat transfer in a single forward-facing step. By using laser Doppler measurement, Armaly *et al.* [4] numerically and experimentally investigated the efficacy of Reynolds number on reattachment length of flow over a backward-facing step inside a rectangular micro-channel and concluded that, reattachment length of flow increases with the increment of Reynolds number. Lee and Matteescu [5] experimentally and numerically investigated 2-D air-flow at Reynolds numbers less than 3000 over a backward-facing step and evaluated the separation and reattachment lengths at the top and bottom of the tube by employing a heated wire with expansion ratios of 1.17 and 2. They observed results similar to those in the previous experimental studies regarding separation and reattachment length at the top and bottom wall of the tube. Separation and reattachment regions of different fluid-flow over the backward and forward-facing arrangements were investigated by numerous researchers [6-12], and they achieved similar results.

By employ ing k-ε model, Yilmaz and Oztop [13] numerically investigated the turbulent flow and heat transfer on a double forward-facing step where the bottom of the wall was heated, and the top of wall and steps were insulated. They figured out that, step ratio had a more considerable influence on heat transfer improvement than length ratio. Oztop *et al.* [14] numerically studied the turbulent flow and heat transfer over a double forward-facing step with a barrier in which the top of the wall was isolated, and the bottom of the wall and steps were heated. They concluded that the aspect ratio of barrier, Ar, had a considerable influence on heat transfer augmentation, and the highest Nusselt number was achieved at $Ar = 1$. Neary and Sotiropoulos [15] numerically studied the laminar fluid-flow inside a 90° diversion rectangular cross-section and indicated that the augmentation of the aspect ratio of the tube had a considerable influence on the flow domain. Barbosa *et al.* [16] numerically studied 3-D mixed and laminar fluid-flow over a backward-facing step with the finite volume method and indicated that, with the increase of Richardson number, the size of primary circulation area decreased.

In the recent past, the nanofluids were widely considered in heat transfer research because of their features. Compared to micron-sized particles, nanoparticles have more surface areas and potential in heat transfer augmentation. Hence, nanofluids can be used in the designing of smaller and lighter heat exchangers.

Abu-Nada [17] studied the laminar flow of nanofluids with different nanoparticles, including Cu, Ag, Al_2O_3, CuO, and TiO_2 of 0-2% volume fractions at Reynolds numbers of 200-600 in the backward-facing step. He found that, in the circulation areas, the use of comparatively lower thermal conductive TiO_2 nanoparticles, the Nusselt number can still be improved. Kherbeet *et al.* [18] investigated the laminar nanofluid-flow in a micro-scale backward-facing step and observed that, with the decreasing of nanoparticles diameter, Nusselt number enhances significantly.

The purpose of this study is to investigate momentum transfer and heat transfer enhancement in an annular channel with abrupt contraction via SST k-ω turbulence model and compare the obtained results with the results of previous studies in this field.

Numerical methods

Geometrical dimensions

Figure 1 represents the sectional diagram of the test section configuration, flow phenomena, and the heat flux on the geometry. The model pattern and meshing process were performed by ANSYS ICEM, which was exported to ANSYS FLUENT, fig. 2. The diameter and length of the outer cylinder of the central pipe are 100 mm of 1000 mm, respectively. Also, the diameters of the outer cylinder of the exit pipe are 100 mm, 80 mm, 60 mm, and 50 mm with a length of 1500 mm. Both entrance and exit pipes are heated under uniform heat flux. The inner tube has a constant diameter and length of 25 mm and 2500 mm, respectively and it is insulated.

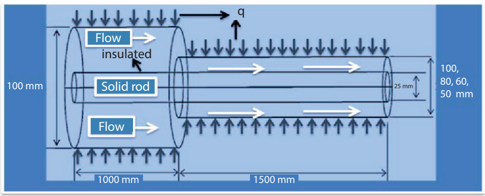

Figure 1. Schematic of geometry

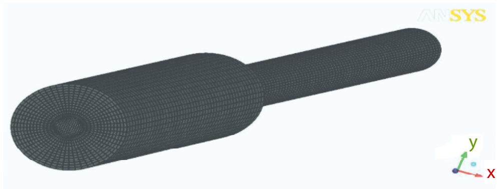

Figure 2. Geometry meshing

Boundary conditions

In the current numerical simulation, the applied boundary conditions were varied from Reynolds numbers of 10000-40000, contraction ratios of 1-2, heat flux of 6000 W/m^2 and TiO_2 nanoparticles volume fractions of 0.5%, 1%, 1.5%, and 2% in water as the base fluid. Uniform inlet velocity was considered for the inlet section of the entrance pipe. Outlet pressure boundary condition was applied to the outlet section of the discharge pipe. According to the energy and Reynolds averaged Navier-Stokes equations, an iteration of SST k-ω viscous model was employed in the present simulation, which provided appropriate solutions for incompressible, steady and turbulent flow near-wall treatment. To obtain accurate results, the second-order upwind method was utilized, based on the finite volume cell faces. Further, for coupling velocity and pressure equations, the SIMPLE algorithm was employed.

Governing equations

In the current simulation, the continuity, momentum, energy and turbulence equations, eqs. (1)-(4), are presented sequentially [19]:

$$\rho \frac{\partial}{\partial x_i}(u_i) = 0 \tag{1}$$

$$\rho \frac{\partial}{\partial x_j}\left(u_i u_j\right) = -\frac{\partial P}{\partial x_i} + \frac{\partial}{\partial x_i}\left[\mu\left(\frac{\partial u_i}{\partial x_j} + \frac{\partial u_j}{\partial x_i}\right)\right] + \frac{\partial}{\partial x_j}\left(-\rho \overline{u_i' u_j'}\right) \tag{2}$$

$$\frac{\partial}{\partial x_i}\left[u_i\left(\rho E\right) + P\right] = \frac{\partial}{\partial x_j}\left[\left(\lambda + \frac{c_p \mu_t}{\mathrm{Pr}_t}\right)\frac{\partial T}{\partial x_j} + u_i (\tau_{ij})_{\mathrm{eff}}\right] \tag{3}$$

where $E = T + (u^2/2)$, and $(\tau_{ij})_{\mathrm{eff}}$ are the deviatory stress tensor:

$$(\tau_{ij})_{\mathrm{eff}} = \mu_{\mathrm{eff}}\left(\frac{\partial u_j}{\partial x_i} + \frac{\partial u_i}{\partial x_j}\right) \tag{4}$$

The equations of the SST k-ω model presented by Menter [20] and applied by Klinzing and Sparrow [21], Tseng *et al.* [22], and Lancial *et al.* [23], can be presented:

$$\rho\left[\frac{\partial}{\partial x_i}(ku_i)\right]=\frac{\partial}{\partial x_j}\left(\Gamma_k\frac{\partial k}{\partial x_j}\right)+G_k-Y_k \tag{5}$$

$$\rho\left[\frac{\partial}{\partial x_i}(\omega u_i)\right]=\frac{\partial}{\partial x_j}\left(\Gamma_\omega\frac{\partial \omega}{\partial x_j}\right)+G_\omega-Y_\omega+D_\omega \tag{6}$$

The effective diffusivity Γ_k and Γ_ω can be written:

$$\Gamma_k=\mu+\frac{\mu_t}{\sigma_k},\quad \Gamma_\omega=\mu+\frac{\mu_t}{\sigma_\omega} \tag{7}$$

where μ_t is given:

$$\mu_t=\propto^*\frac{\rho k}{\omega} \tag{8}$$

and $\propto^*$ is a coefficient for damping the turbulent viscosity which can be calculated as follow eq. (9):

$$\propto^*=\propto^*_\infty\frac{\left(\propto^*_0+\frac{\mathrm{Re}_t}{R_k}\right)}{\left(1+\frac{\mathrm{Re}_t}{R_k}\right)} \tag{9}$$

The coefficients in eq. (9) are, $\mathrm{Re}_t=\rho k/\mu\omega$, $\propto^*_0=\beta_1/3$:

$$\beta_i=F_1\beta_{i,1}+(1-F_1)\beta_{i,2} \tag{10}$$

The turbulent Prandtl numbers of k and ω can be calculated [24]:

$$\sigma_k=\frac{1}{\frac{F}{\sigma_{k,1}}+\left[\frac{1-F_1}{\sigma_{k,2}}\right]} \tag{11}$$

$$\sigma_\omega=\frac{1}{\frac{F_1}{\sigma_{\omega,1}}+\left[\frac{1-F_1}{\sigma_{\omega,2}}\right]} \tag{12}$$

The blending function, F_1, is calculated:

$$F_1=\tan h\left(\Phi_1^4\right) \tag{13}$$

where

$$\Phi_1=\min\left[\max\left(\frac{\sqrt{k}}{0.09\omega y}\frac{500\mu}{\rho y^2\omega}\right),\frac{4\rho k}{\sigma_{\omega,2}D^+_\omega y^2}\right] \tag{14}$$

and

$$D^+_\omega=\max\left[2\rho\frac{1}{\sigma_{\omega,2}}\frac{1}{\omega}\frac{\partial k}{\partial x_i}\frac{\partial \omega}{\partial x_j},10^{-10}\right] \tag{15}$$

where D_ω^+ is the positive portion of the cross-diffusion term.

The G_k indicates turbulent kinetic energy generation by average velocity gradients and G_ω suggests the production of ω and D_ω in-cross diffusional terms:

$$D_\omega = 2\left(1-F_1\right)\rho\sigma_{\omega,2}\frac{1}{\omega}\frac{\partial k}{\partial x_j}\frac{\partial \omega}{\partial x_i} \tag{16}$$

The Y_k and Y_ω show the dissipations of k and ω because of turbulence:

$$Y_k = \rho\beta^* k\omega \tag{17}$$

$$Y_\omega = \rho\beta_i\omega^2 \tag{18}$$

The G_k can be written:

$$G_k = \tau_{t,ij}\frac{\partial u_i}{\partial u_j} \tag{19}$$

where

$$\tau_{t,ij} = \mu_t\left(\frac{\partial u_i}{\partial x_j}+\frac{\partial u_j}{\partial x_i}\right)-\left(\frac{2}{3}\rho k\delta_{ij}\right) \tag{20}$$

The G_ω is also a function of G_k:

$$G_\omega = \frac{\rho\alpha}{\mu_t}G_k \tag{21}$$

where $\propto$ can be obtained:

$$\propto = \left(\frac{\alpha_\infty}{\alpha^*}\right)\frac{\left(\propto_0^* + \frac{\mathrm{Re}_t}{R_k}\right)}{\left(1+\frac{\mathrm{Re}_t}{R_k}\right)} \tag{22}$$

where $\propto_\infty$ is defined:

$$\propto_\infty = F_1 \propto_{\infty,1} + \left(1-F_1\right)\propto_{\infty,2} \tag{23}$$

where

$$\propto_{\infty,1} = \frac{{}_{,1}}{{}_{\infty}} - \frac{}{\sigma\ {}_{,1}\sqrt{\beta_\infty}} \tag{24}$$

$$\propto_{\infty,2} = \frac{\beta_{i,2}}{\beta_\infty^*} - \frac{k^2}{\sigma_{\omega,2}\sqrt{\beta_\infty^*}} \tag{25}$$

Table 1 presents the constants of the SST k-ω model

Table 1. Coefficients for the SST *k*-*ω* turbulent model [22]

$\sigma_{k,1} = 1.176$	$\sigma_{k,2} = 1$	$\sigma_{\omega,1} = 2$	$\sigma_{\omega,2} = 1.168$	$\beta_{i,1} = 0.075$
$\beta_{i,2} = 0.0828$	$R_k = 6$	$k = 0.41$	$\beta_\infty^* = 0.09$	

Thermophysical properties of nanofluids

The effective density of nanofluid, ρ_{nf}, based on Vajjha and Das [25] equation:

$$\rho_{\mathrm{nf}} = (1-\phi)\rho_{\mathrm{f}} + \phi\rho_{\mathrm{np}} \tag{26}$$

where ρ_f and ρ_{np} indicate the density of carrying fluid and nanoparticles, respectively.

The specific heat capacity of nanofluid can be obtained:

$$(\rho c_p)_{\mathrm{nf}} = (1-\phi)(\rho c_{\mathrm{p}})_{\mathrm{f}} + \phi(\rho c_p)_{\mathrm{np}} \tag{27}$$

where $(\rho c_p)_{\mathrm{f}}$ and $(\rho c_p)_{\mathrm{np}}$ are the specific heat capacities of the carrying fluid and the nanoparticles, respectively.

The efficient thermal conductivity of the solid-liquid mixtures presented by Xuan and Roetzel [26] and Wang *et al.* [27]:

$$k_{\mathrm{eff}} = k_{\mathrm{f}}\left[\frac{k_{\mathrm{p}} + 2k_{\mathrm{f}} - 2\phi(k_{\mathrm{f}} - k_{\mathrm{p}})}{k_{\mathrm{p}} + 2k_{\mathrm{f}} + \phi(k_{\mathrm{f}} - k_{\mathrm{p}})}\right] \tag{28}$$

According to Brickman [28], the viscosity of the suspension correlates with the concentration of the particles in the suspension:

$$\mu_{\mathrm{eff}} = \frac{\mu_{\mathrm{f}}}{(1-\phi)^{2.5}} \tag{29}$$

This equation is used for low volume fractions of the particles in the suspension ($\phi < 0.05$).

Numerical procedure

The ANSYS 14 ICEM software was used to generate the computation mesh while the heat transfer and flow equations were solved by ANSYS-FLUENT 14. For obtaining the precise mesh, the ICEM tools for dealing with complex geometry were utilized. The SST *k-ω* model was employed to analyze the heat transfer and TiO_2 nanofluid-flow in the annular space between two concentric cylinders. To investigate grid independence, the stepwise grid sizes were considered, and the data were compared until the differences became minimal, which could be ignored. An annular channel without step, $CR = 1$, Re = 10000, and pure water was allowed to flow with the varied flow velocity. Five sizes of grids were considered to conduct a grid independence study where the fourth grid represented grid independence because the difference between the fifth and the fourth grids was less than 1, tab. 2.

Table 2. Grid independent test for pure water at *CR* = 1 and Re = 10000

Grid No.	Size of mesh	Have
1	$X = 20$, $Y = 20$, $Z = 350$	744.67890
2	$X = 20$, $Y = 20$, $Z = 500$	748.15942
3	$X = 20$, $Y = 20$, $Z = 750$	749.07886
4	$X = 20$, $Y = 20$, $Z = 1000$	749.70679
5	$X = 20$, $Y = 20$, $Z = 1150$	749.71155

In this study, the data of turbulent flow and heat transfer over a double forward-facing step, the efficacy of the height of step of Oztop *et al.* [1] were considered for validation of the generated results. According to fig. 3, the present model is in a reasonable compromise with the numerical data of Oztop *et al.* [14]. Here the presently obtained values for Nusselt number are compared with the results of Oztop *et al.* [14] for the previously described specific Case 1, at Re = 30000 and $T = 313$ K. It can be observed that the velocity profile is comparable, as the velocity was overestimated by about 3%. Further, for the turbulent flow, heat transfer to air-flow in an annular channel with sudden contraction by Togun *et al.* [29] was simulated, and the numerical results are presented in fig. 4. Here the present results could be compared with the data of Togun *et al.* [29] for contraction ratio of $CR = 2$ and $q = 4000$ W/m^2, and it can be seen that the results of the current simulation are agreed with the data of Togun *et al.* [29].

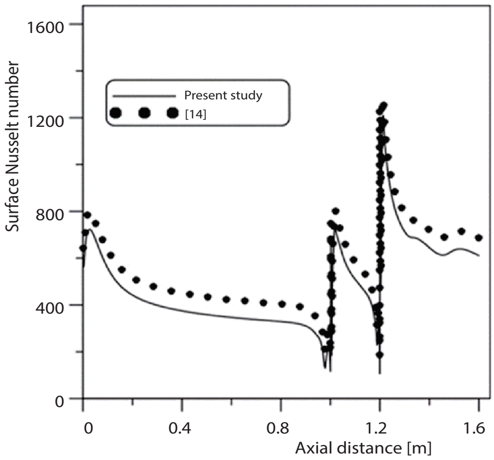

Figure 3. Comparison of Nusselt number with Oztop *et al.* [14]

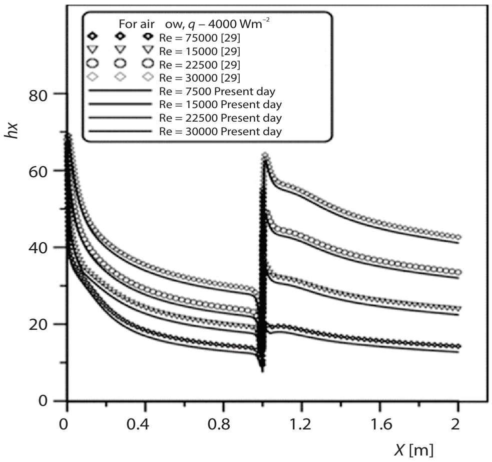

Figure 4. Comparison of heat transfer coefficient with Togun *et al.* [29]

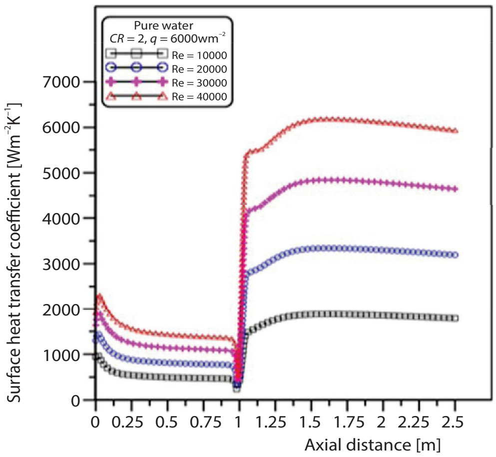

Figures 5. Variations of surface heat transfer coefficient for pure water at *CR* = 2 and different Reynolds number

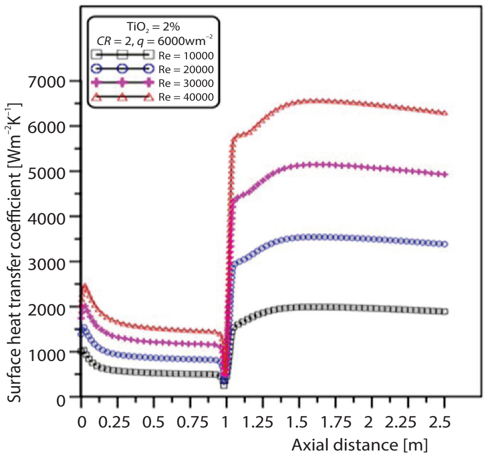

Figure 6. Variations of surface heat transfer coefficient for TiO_2 nanofluid at *CR* = 2 and different Reynolds number

Results and discussion

Here, the efficacy of Reynolds number, nanoparticles volume fraction, and contraction ratio on surface heat transfer coefficient and pressure drop are analyzed and illustrated.

Influence of Reynolds number

Profile of surface heat transfer coefficient for pure water and suspension of water at 2% TiO_2 nanoparticles at different Reynolds numbers and a contraction ratio of 2 are presented in figs. 5 and 6, respectively. It is observed that the profile of surface heat transfer decreases gradually before the reduction of the passage but suddenly increases after the step due to the increase of flow rate and pressure drop. In general, the rising of Reynolds number enhances the heat transfer coefficient, and the highest value was obtained at 2% TiO_2 nanoparticles volume fraction in water compared with the data collected for distilled water. Generally, fluid velocity plays a significant role in thermal performance, especially for forced convection, where the heat transfer coefficient enhances with the increase of Reynolds number.

Effect of contraction ratio

Figure 7 and 8 present the influence of contraction ratio on the surface heat transfer coefficient for 2% TiO_2 nanoparticles volume fraction and pure water at Re = 40000 and heat flux of 6000 W/m^2. According to the obtained numerical results in all the cases, the surface heat transfer coefficient profile manifests the same trend at the entrance pipe, whereas the differences between heat transfer coefficient graphs are dependent on the difference in contraction passage of channel. The selected graphical presentations represent the efficacy of the height of the step on the surface heat transfer coefficient. Re-circulation flow, which was created before and after the step, has a significant influence on the surface heat transfer coefficient. In the present investigation, the highest value of heat transfer enhancement was obtained at the contraction ratio of 2.

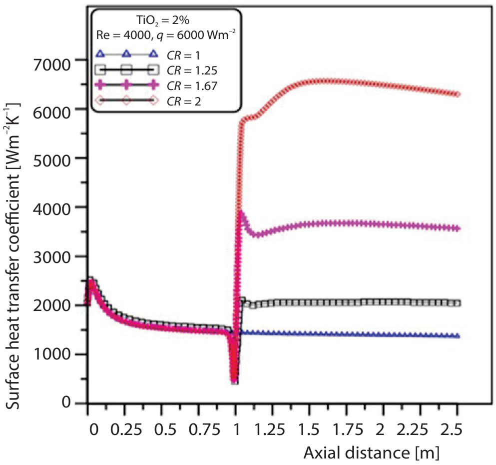

Figures 7. Effect of contraction ratio on surface heat transfer coefficient for 2% TiO_2 nanofluid at Re = 40000 and q = 6000 W/m^2

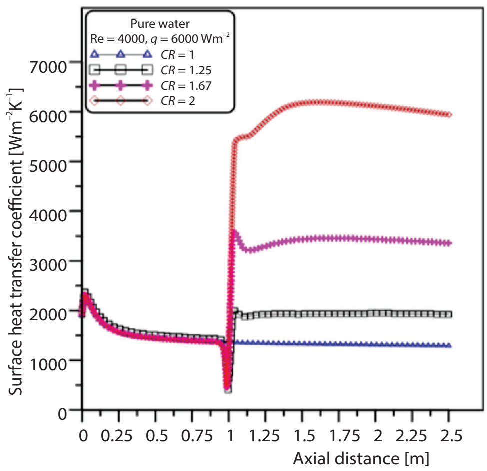

Figure 8. Effect of contraction ratio on surface heat transfer coefficient for pure water at Re = 40000 and q = 6000 W/m^2

Influence of volume fraction

Figure 9 represents the distribution of surface heat transfer coefficient at various nanoparticles volume fractions (0.5-2%), Re = 40000, and at the contraction ratios of 2. Generally, the enhancement of nanoparticle volume fraction causes the augmentation of the convective heat transfer coefficient from the surface in annular pipe flow with flow passage contraction. Such increment in the heat transfer coefficient is due to the nanofluid thermal conductivity, viscosity improvement, random and migratory movement of nanoparticles, as well as particle-particle collisions and Brownian diffusion. The results demonstrate that the influence of nanoparticles volume fraction with re-circulation flow results in higher thermal performance, and the highest value of heat transfer coefficient in the present investigation were obtained at 2% TiO_2 volume fraction compared to others.

Influence of heat flux

Figure 10 presents the distribution of surface heat transfer coefficients for 2% TiO_2 nanoparticles volume fraction at Re = 40000 and contraction ratio of 2. It can be seen that there is no remarkable increase in surface heat transfer coefficients with the enhancement of heat flux. Heat transfer coefficients prevail a similar trend in this case.

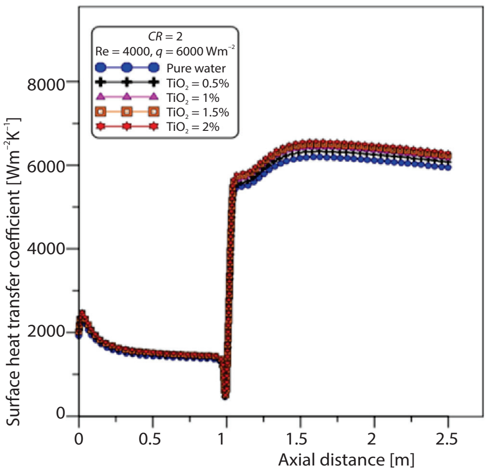

Figure 9. Effect of volume fraction on the surface heat transfer coefficient for *CR* = 2 at Re = 40000, and *q* = 6000 W/m²

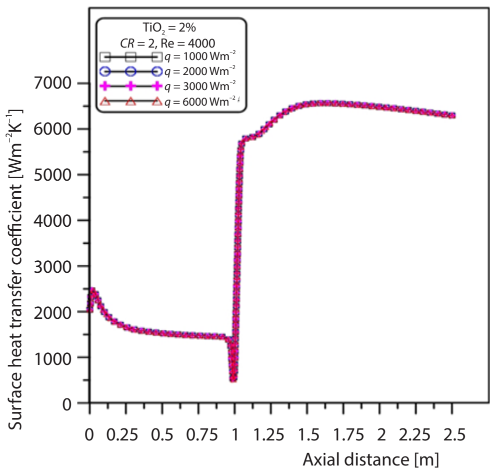

Figure 10. Effect of heat flux on the surface heat transfer coefficient for TiO_2 at Re = 40000, and *CR* = 2

Pressure drop

Variations of pressure drop for the suspension of 2% TiO_2 volume fraction at Re = 40000 and different contraction ratios are illustrated in fig. 11. Results show that the pressure drop suddenly decreases and increases before and after the step, respectively, due to re-circulation flow created by hydrodynamic fluid-flow through the channel. The effects of Reynolds number on pressure drop at 2% TiO_2 volume fraction and contraction ratio of 2 are presented in fig. 12. Pressure drop enhances with the augmentation of Reynolds number, and the highest value of pressure drop is obtained at the highest value of Re = 40000 compared to others in the present range of investigation.

Velocity distribution

Figures 13 and 14 show the velocity distribution at five positions before and after the step at Re = 40000 and contraction ratio of 2. The fully developed velocity with two circulation areas is observed before and after the step, where the size of the re-circulation area is appeared to decrease with the increasing distance from the step. The re-circulation flow profiles before the step are close to one side of the wall, while after the step, they are almost axisymmetric on channel walls. The effect of contraction ratio on velocity profile at 99 cm before the step and 101 cm after the step for Re = 40000 is presented in figs. 15 and 16. The velocity distribution looks changed with the increase of contraction ratio owing to the re-circulation areas generated before and after the step, which affects raising the thermal performance. In both the cases of

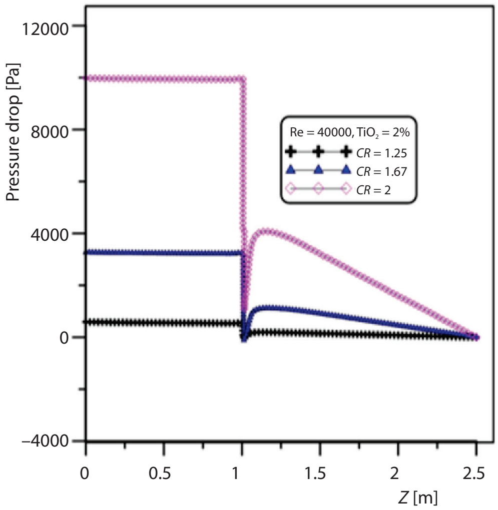

Figure 11. Variations of pressure drop for 2% of TiO_2 nanofluid at different contraction ratio

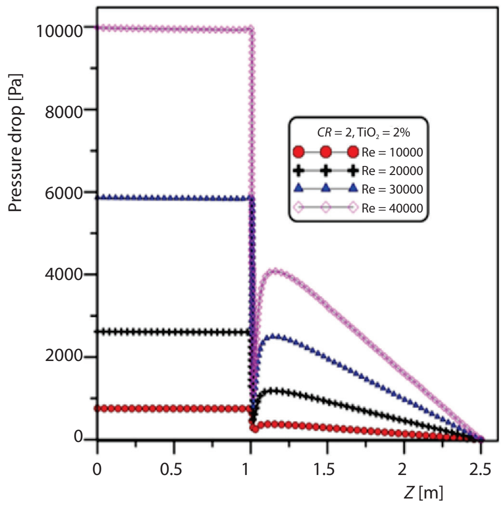

Figure 12. Variations of pressure drop for 2% of TiO_2 nanofluid at different Reynolds number

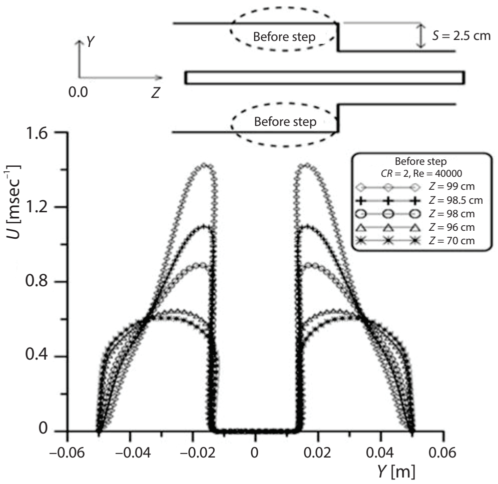

Figures 13. Velocity distributions at *CR* = 2 and Re = 40000 for different positions before the step

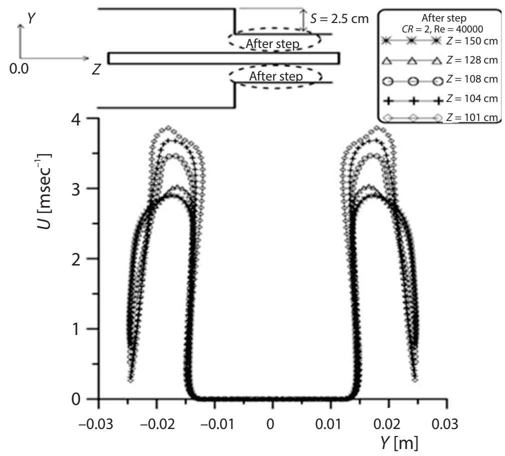

Figure 14. Velocity distributions at *CR* = 2 and Re = 40000 for different before positions after the step

before and after contraction, the maximum re-circulation flow is seen at the contraction ratio of 2, compared with the other cases.

Conclusio

In this 3-D numerical investigation, flow and heat transfer in the annular space between two concentric cylinders with abrupt contractions were considered. The influence of Reynolds number and contraction ratio on the surface heat transfer coefficient and the increment of heat transfer coefficient were investigated. The maximum heat transfer improvement was observed at the contraction ratio of 2 in the investigated range. The enhancement of heat transfer occurred due to the development of re-circulation flow before and after the step. The

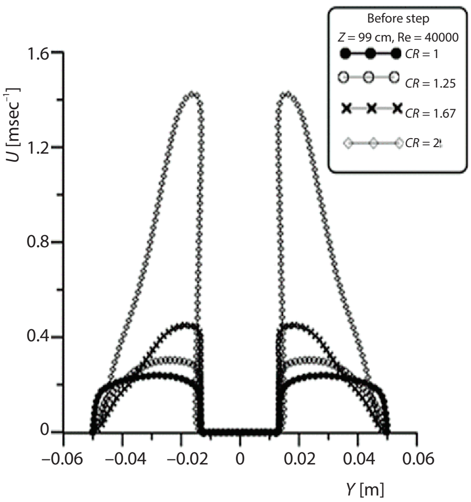

Figure 15. Effect of contraction ratio on velocity distributions before the step at Z = 99 cm for Re = 40000

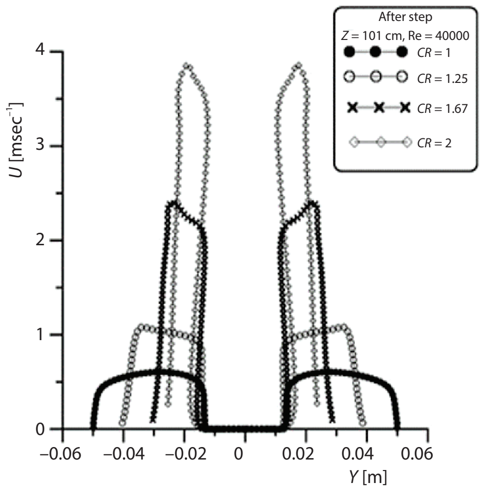

Figure 16. Effect of contraction ratio on velocity distributions after the step at Z = 101 cm for Re = 40000

influence of nanoparticle volume fraction on the improvement of the heat transfer coefficient was investigated and observed that at 2% TiO_2 volume fraction, the heat transfer enhancement was the highest compared with water data in the investigation range. It could be inferred that the two circulation areas observed before and after the step was the main reason for the improvement in the heat transfer rate. With the increase of the Reynolds number and contraction ratio, the pressure drop enhances and then drops with the distance before the step and gradually increases after the step in all cases.

Nomenclature

a	– entrance pipe length, [m]	Nu	– Nusselt number
b	– exit pipe length, [m]	P	– pressure, [Pa]
c_p	– specific heat capacity, [J kg^{-1}K^{-1}]	Pr	– Prandtl number
CR	– contraction ratio (= D_e/D_t)	q	– heat flux, [Wm^{-2}]
D_e	– entrance pipe diameter, [m]	Re	– Reynolds number
D_i	– inner pipe diameter, [m]	S	– step height, [m]
D_t	– exit pipe diametr	T	– temperature, [K]
E	– total energy, [Jkg^{-1}]	U	– velocity component, [ms^{-1}]
hx	– heat transfer coefficient, [Wm^{-2}K^{-1}]	X_i	– upstream length, [m]
k	– turbulent kinetic energy, [m^{2}s^{-2}]	X, Y, Z	– Cartesian co-ordinates, [m]

References

[1] Abu-Mulaweh, H. I., Turbulent Mixed Convection Flow over a Forward-Facing Step the Effect of Step Heights, *International Journal of Thermal Sciences*, *44* (2005), 2, pp. 155-162
[2] Orselli, R. M., de Lemos, M. J. S., Sudden Contraction in a Turbulent with a Porous Insert, *Latin American Journal of Solids and Structures*, *2* (2005), pp. 269-290
[3] Gandjalikhan Nassab, S. A., *et al*., Turbulent Forced Convection Flow Adjacent to Inclined Forward Step in a Duct, *International Journal of Thermal Sciences*, *48* (2009), 7, pp. 1319-1326
[4] Armaly, B. F., *et al*., Experimental and Theoretical Investigation of Backward-Facing Step Flow, *Journal of Fluid Mechanics*, *127* (2006), Feb., pp. 473-496
[5] Lee, T., Mateescu, D., Experimental and Numerical Investigation of 2-D Backward-Facing Step Flow, *Journal of Fluids and Structures*, *12* (1998), 6, pp. 703-716

[6] Oon, C. S., *et al.*, Computational Simulation of Heat Transfer to Separation Fluid-Flow in an Annular Passage, *International Communications in Heat and Mass Transfer*, *46* (2013), Aug., pp. 92-96
[7] Oon, C. S., *et al.*, Numerical Simulation of Heat Transfer to Separation Air-Flow in an Annular Pipe, *International Communications in Heat and Mass Transfer*, *39* (2012), 8, pp. 1176-1180
[8] Kazi, S. N., *et al.*, Heat Transfer to Separation Flow in Heat Exchangers, in: *An Overview of Heat Transfer Phenomena*, IntechOpen, Rijeka, Croatia, 2012
[9] Togun, H., Laminar CuO-water Nanofluid-Flow and Heat Transfer in a Backward-Facing Step with and without Obstacle, *Applied Nanoscience*, *6* (2016), 3, pp. 371-378
[10] Togun, H., *et al.*, Numerical Study of Turbulent Heat Transfer in Annular Pipe with Sudden Contraction, *Applied Mechanics and Materials*, *465-466* (2014), Jan., pp. 461-466
[11] Togun, H., *et al.*, An Experimental Study of Heat Transfer to Turbulent Separation Fluid-Flow in an Annular Passage, *International Journal of Heat and Mass Transfer*, *54* (2011), 4, pp. 766-773
[12] Togun, H., *et al.*, The CFD Simulation of Heat Transfer and Turbulent Fluid-flow over a Double Forward-Facing Step, *Mathematical Problems in Engineering*, *2013* (2013), ID895374
[13] Yılmaz, I.I., Oztop, H. F., Turbulence Forced Convection Heat Transfer over Double Forward Facing Step Flow, *International Communications in Heat and Mass Transfer*, *33* (2006), 4, pp. 508-517
[14] Oztop, H. F., *et al.*, Analysis of Turbulent Flow and Heat Transfer over a Double Forward Facing Step with Obstacles, *International Communications in Heat and Mass Transfer*, *39* (2012), 9, pp. 1395-1403
[15] Neary, V. S., Sotiropoulos, F., Numerical Investigation of Laminar Flows through 90-degree Diversions of Rectangular Cross-Section, *Computers and Fluids*, *25* (1996), 2, pp. 95-118
[16] Barbosa Saldana, J. G., *et al.*, Numerical Simulation of Mixed Convective Flow over a 3-D Horizontal Backward Facing-Step, *Journal of Heat Transfer*, *127* (2005), 9, pp. 1027-1036
[17] Abu-Nada, S., Experimental Investigation of Natural-Convection Heat Transfer in Horizontal and Inclined Annular Fluid Layers, *Heat Mass Transfer*, *44* (2008), Sept., pp. 929-936
[18] Kherbeet, A. S., *et al.*, The Effect of Nanofluids Flow on Mixed Convection Heat Transfer over Microscale Backward-Facing Step, *International Journal of Heat and Mass Transfer*, *55* (2012), 21-22, pp. 5870-5881
[19] Manca, O., *et al.*, A Numerical Study of Nanofluid Forced Convection in Ribbed Channels, *Applied Thermal Engineering*, *37* (2012), May, pp. 280-292
[20] Menter, F. R., Two-Equation Eddy-Viscosity Turbulence Models for Engineering Applications, *AIAA Journal*, *32* (1994), 8, pp. 1598-1605
[21] Klinzing, W. P., Sparrow, E. M., Evaluation of Turbulence Models for External Flows, Numerical Heat Transfer – Part A: *Applications*, *55* (2009), 3, pp. 205-228
[22] Tseng, Y. S., *et al.*, Investigating Flow and Heat Transfer Characteristics in a Fuel Bundle with Split-Vane Pair Grids by CFD Methodology, *Annals of Nuclear Energy*, *64* (2014), Feb., pp. 93-99
[23] Lancial, N., *et al.*, Effects of a Turbulent Wall Jet on Heat Transfer over a Non-Confined Backward-Facing Step, *International Journal of Heat and Fluid-Flow*, *44* (2013), Dec., pp. 336-347
[24] Dutta, R., *et al.*, Comparison of Various Integration Wall (ITW) RANS Models for Predicting Turbulent Slot Jet Impingement Heat Transfer, *International Journal of Heat and Mass Transfer*, *65* (2013), pp. Oct., 750-764
[25] Vajjha, R. S., Das, D. K., Experimental Determination of Thermal Conductivity of Three Nanofluids and Development of New Correlations, *International Journal of Heat and Mass Transfer*, *52* (2009), 21-22, pp. 4675-4682
[26] Xuan, Y., Roetzel, W., Conceptions for Heat Transfer Correlation of Nanofluids, *International Journal of Heat and Mass Transfer*, *43* (2000), 19, pp. 3701-3707
[27] Wang, B.-X., *et al.*, Research on the Heat-Conduction Enhancement for Liquid with Nanoparticle Suspensions, General Paper (G-1), *Proceedings*, International Symposium on Thermal Science and Engineering (TSE2002), Beijing, China, 2000
[28] Brinkman, H. C., The Viscosity of Concentrated Suspensions and Solutions, *The Journal of Chemical Physics*, *20* (1952), 4, pp. 571-571
[29] Abdulrazzaq, T., *et al.*, Heat Transfer and Turbulent Fluid-Flow over Vertical Double Forward-Facing Step, World Academy of Science, *Engineering and Technology*, *86* (2014), pp. 722-726

Paper submitted: July 9, 2018
Paper revised: July 25, 2019
Paper accepted: August 8, 2019